



Investigation of the friction conditions of self-pierce rivets by means of a compression-torsion tribometer

Moritz Rossel¹ · Gerson Meschut¹

Received: 25 January 2022 / Accepted: 9 March 2022 / Published online: 13 April 2022
© The Author(s) 2022

Abstract

Lightweight design is an effective lever for achieving fuel consumption and emission-oriented goals. Therefore micro-alloyed steels and high-strength aluminium materials are included in the multi-material mix of the car body. In this context self-pierce riveting has become established for joining in body-in-white production. For the dimensioning of the joint, numerical simulation is increasingly being used. In order to make reliable predictions about joint quality, knowledge of the friction in the joining process is necessary and needs to be identified experimentally. In previous investigations, the process parameters in the friction test were not comparable to the joining process. Therefore, a new friction test method is presented in this paper, where the process conditions are comparable between joining and friction testing especially regarding the interface pressure. The local joining process parameters between rivet and sheet are derived numerically. In the framework of the investigations, the influences of the local joining process parameters, like interface pressure, relative velocity and temperature, on the friction are investigated and mapped close to the joining process. Additionally a comparison of different rivet coatings is carried out. The rivet contact to the sheet metal HX340LAD as well with aluminium EN AW-5182 is taken into account.

Keywords Self-pierce riveting · Simulation · Friction · Coating · Tribology

1 Introduction

Environmental protection is one of the major challenges for modern industrial production. Driven by restrictive laws and customer requirements for low-emission mobility, the automotive industry is trying to reduce greenhouse gas emissions. In addition to reducing CO₂-emissions from conventional drive technologies, electro mobility is also being consistently pursued. In this context, lightweight design plays a key role in terms of range. Due to lightweight construction, new materials are continuously being introduced into body-in-white production. Thereby self-pierce riveting has established itself in series production for joining steel and aluminium alloys. In order to estimate the load-bearing capacity, joining process simulations are carried out to predict the characteristic joint geometry. This requires knowledge of the friction in the joining process, as this correlates strongly with joint quality [1]. The investigation of Li [2]

confirmed this for different surface treatment processes of aluminium sheets. Furthermore the friction between the rivet and the sheet metal influences the undercut of the joint [3]. Ang mentioned, the significant influence of friction on the load-bearing joint capacity [4]. The coating of the rivet can reduce the friction between rivet and sheet metal. Thus, the rivet coating correlates directly with the load-bearing capacity of the joint. This was confirmed by the investigations of Karim et al. [5], where higher friction coefficients were identified for ALMAC[®] than for ZnNi + B18, which resulted in a higher joint strength. The micro-mechanical friction test used by Karim et al. [5] showed a high fluctuation range of the friction values and can rather be interpreted as a qualitative test. A stationary state did not develop during the friction test.

As described in Wituschek et al. [6], there are two relevant tribological systems in which the rivet is involved. In past publications, the friction between rivet and sheet metal at very low interface pressures compared to the joining process have already been investigated. Interface pressures up to 6 MPa were investigated in Wituschek et al. [6], but since semi-tubular self-piercing riveting is a joining by forming process, interface pressures above the yield stress

✉ Moritz Rossel
moritz.rossel@lwf.upb.de

¹ Laboratory for Material and Joining Technology, Paderborn University, Pohlweg 47-49, 33098 Paderborn, Germany

of the materials occur. The aim of this paper is to tailor the process parameters in the friction test analogously to the joining process especially in terms of interface pressure. Furthermore, the friction test should be able to parameterize complex friction models by an independent choice of process parameters. To evaluate the process parameters in the joining process, an inverse determination is carried out by means of numerical simulation, whereby a subroutine automatically evaluates the nodes in the contact between the joining part and the rivet. Thereon, the influence of the process parameters on friction is investigated experimentally and interpreted in detail. For this purpose a friction test bed from a recent work is used and extended for the application of joining elements [7].

2 Materials and methods

In the following chapters, the boundary conditions of the experimental and numerical investigations are presented.

2.1 Mechanical behaviour of materials and coatings

A micro-alloyed steel (HX340LAD) and a high-strength aluminium alloy of the 5000 series (EN AW-5182) with a thickness of 1.5 mm are used as joining partners. The mechanical properties of the sheet metal materials are located in Table 1.

The steel material HX340LAD is provided with a hot-dip galvanized zinc coating that has a thickness of up to 10 μm . The aluminium EN AW-5182 is titanium-zirconium coated and intended for visible parts in automotive industry.

For the joints, a C-rivet of type C5.3 \times 5.0 H4 and a flat die of type FM0902218 from Wilhelm Böllhoff GmbH &

Co. KG is used. The rivets are made of quenched and tempered steel 38B2 and have a hardness class of four according to DVS3410. This corresponds to a hardness of 480 ± 30 HV. Within the scope of the investigations, rivets with an ALMAC[®]- as well as with a ZnNi + B18-coating are considered. The ALMAC[®]-coating is consisting of zinc, tin and aluminium, which is applied by mechanical plating [8]. The ZnNi + B18-coating is galvanic applied and generates maximum corrosion resistance with 10–15% nickel and a chrome topcoat [9]. Both coatings have a thickness of 10–12 μm on the rivet head and shank. Figure 1 shows the roughness of the coatings. It can be seen that the ALMAC[®]-coating has a slightly higher roughness depth Rz than ZnNi + B18. The ZnNi + B18-coating has a hardness of 462.59 HV0.05. The ALMAC[®]-coating is significantly softer at 359.51 HM. A measurement of the vicker hardness was not feasible due to the low hardness.

The experimentally determined yield curve of the sheet metal material HX340LAD is extrapolated by Ludwik. The yield curve of the sheet metal material EN AW-5182 and rivet material 38B2 are extrapolated according to Voce. As can be seen in an earlier publication, the temperature dependence of the yield stress can be neglected e.g. for HX340LAD due to a very small deviation in a single-digit percentage range for up to 200 °C [10]. All extrapolations are validated by layer compression tests and are depicted in Fig. 2.

2.2 Methods and procedures

In this paper, two material thickness combinations are under investigation as shown in Table 2. Derived from the table there are two contact combinations including the rivet which are relevant for the joining process.

For the experimental friction tests, the test bed shown in Fig. 3 based on a compression-torsion-tribometer is used. In order to reproduce the high interface pressures from the joining process, this test bed is required. Furthermore, the kinematic enables an independent process parameter setting, so complex friction models can be parameterized.

In Rossel et al. [11], this friction test was used for pure joining part contact in clinching. This paper presents an advancement to the contact between self-pierce rivet and sheet metal.

Table 1 Mechanical properties of the used sheet metal materials (R_e = Yield point in (MPa), R_m = Tensile Strength in (MPa), A_{80} = Elongation at break in (%))

Material	R_e	R_m	A_{80}
HX340LAD	390.93	467.37	25
EN AW-5182	145.02	290.57	25

Fig. 1 Roughness parameters R_a and R_z of the rivet coatings ALMAC[®] and ZnNi + B18

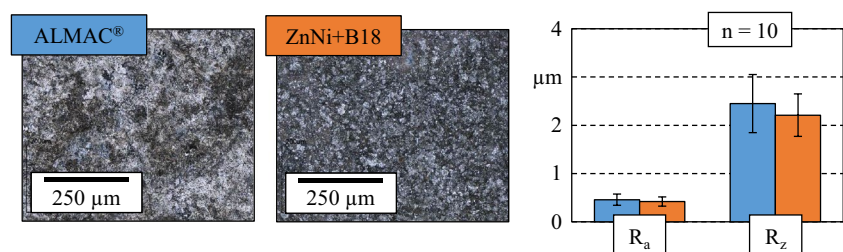


Fig. 2 Yield stress—Plastic strain curves of the materials under consideration

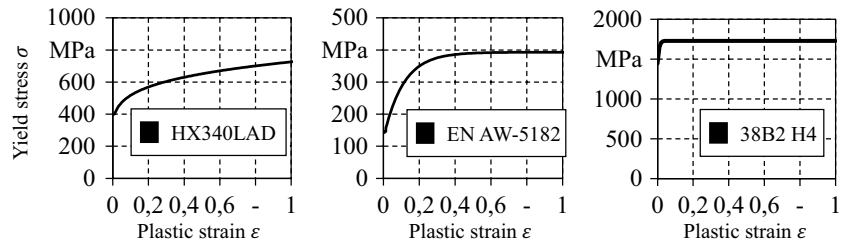


Table 2 Material-thickness-combinations (MTC) under investigation

MTC	Joining partner 1	Joining partner 2
1	EN AW-5182	HX340LAD
2	HX340LAD	EN AW-5182

During the friction test, the rivet is clamped on the shank surface by means of two modular exchangeable jaws. Figure 4 shows that the rivet is secured against rotation by clamping.

For the contact between sheet metal and rivet, the positioning of the specimens to each other is shown in Fig. 5. In the friction test, the two contact partners are pressed axially against each other and frictioned by a rotational movement. Optionally, the temperature of the friction test can be adjusted by a heating coil. An encapsulation of the specimens is not necessary, since the rivet forms locally slightly into the sheet metal without generating failure through radial cracks. The reason for this is the larger specimen diameter of the sheet metal.

The sheet metal specimens are made using a stamping process and have a diameter of 12 mm. The rivet heads have a nominal friction surface of 43.63 mm² and a nominal mean friction radius of 2.48 mm, which is used as a reference for the relative velocity since it is a torsional motion (calculation compare to Rossel et al. [11]) In order to maintain the similarity to the industrial joining process, the sheets and rivets are in delivery condition.

As the illustration shows, the friction test takes place between the rivet head and the sheet metal. This is legitimate, since the coating application on the head and the rivet shank or foot is comparable. The contact in the joining process actually takes place on the rivet shank and the rivet foot. However, since there is no defined, flat surface, the rivet head is frictioned.

For the comparability of the friction properties, the Coulomb friction coefficient is used. The friction coefficient links the interface pressure and the frictional shear stress by the following linear relationship.

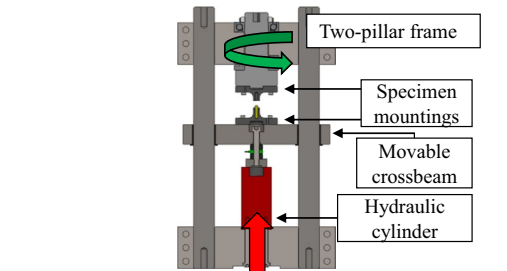


Fig. 3 Schematic illustration of the friction test bed [1]

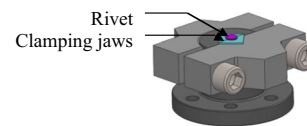


Fig. 4 Clamping concept for auxiliary joining elements in the friction test bed

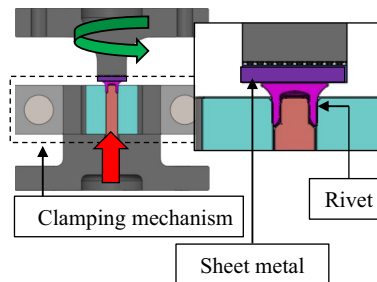


Fig. 5 Positioning of rivet and sheet metal relative to each other in the friction test

$$\mu = \tau_R / \sigma_N \tag{1}$$

The coefficient μ provides easy comparability of coating and influences of the local joining process parameters.

Based on the results of the numerical joining process simulation that will be later presented in Sect. 3.1, the following tests are considered in order to identify the influence of rivet coatings as well as the different process parameters with regard to the frictional behaviour (Tables 3, 4, 5, 6).

Table 3 Parameter field for the experimental friction investigation in terms of interface pressure ($v_{rel} = 10 \text{ mm/s}$; $T = 20 \text{ }^\circ\text{C}$)

Interface pressure (MPa)						
50	150	300	400	500	600	700

Table 4 Parameter field for the experimental friction investigation in terms of relative velocity ($\sigma_N = 50 \text{ MPa}$; $T = 20 \text{ }^\circ\text{C}$)

Relative velocity (mm/s)			
5	10	15	20

Table 5 Parameter field for the experimental friction investigation in terms of temperature ($\sigma_N = 50 \text{ MPa}$; $v_{rel} = 10 \text{ mm/s}$)

Temperature ($^\circ\text{C}$)			
20	50	100	150

Table 6 Different rivet coatings for the experimental friction investigation ($\sigma_N = 50 \text{ MPa}$; $v_{rel} = 10 \text{ mm/s}$; $T = 20 \text{ }^\circ\text{C}$)

Coatings	
ALMAC [®]	ZnNi + B18

2.3 Numerical modelling conditions

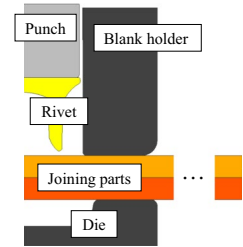
In order to determine the friction-relevant local joining process parameters in the contact between rivet and sheet metal numerical joining process simulations are carried out. For this purpose, a 2D-axis symmetrical joining process is implemented in Simufact.forming 16.0. The joining partners and the rivet were modeled elasto-plastically, whereas the tools are assumed to be rigid. Figure 6 shows the geometric formation of the numerical joining process simulation.

A combined friction law is used, which is implemented via a subroutine for the purpose of simple evaluation of the friction relevant process parameters. A global friction coefficient of $\mu = 0.15$ and a friction factor of $m = 0.4$ are used. The additional friction factor is used to prevent the occurrence of unphysically high frictional shear stresses and to keep the simulation close to reality. Since the joining process simulation has been experimentally validated in terms of the characteristic geometry and the joining force with this frictional parameter set, it can be assumed that the local joining process parameters are realistic.

A geometric criteria was used to model the cut through the upper sheet. Microsections slightly before and after cutting were used to parameterize the criterion. In order to prevent mesh distortion, adaptive remeshing and local refinement were utilized.

The joining speed is 20 mm/s, although this is not constant during joining due to the deceleration prior the bottom dead centre of the joining machine. In order to ensure

Fig. 6 Geometric model of the 2D-axisymmetrical joining process simulation



comparability with the experiment, an experimental joining stroke—joining time curve defines the joining velocity in the simulation. Thus, the relative velocity in the contacts are close to reality. The thermal properties are defined by means of literature values (e.g. according to Piott et al. [12]) and are shown in Table 7.

3 Results and discussion

In the following, the local joining process parameters from the simulation are shown, from which the experimental investigations are derived, which are presented in the subsequent section.

3.1 Numerical investigations

The friction-relevant local joining process parameters are evaluated at four discrete joining stages in the process simulation. An evaluation takes place at 25, 50, 75 and 95% of the maximum joining stroke for both joints. A subroutine writes out the node state variables of the rivet nodes that are in contact with one of the joining partners. For this purpose, a note-to-segment contact is used to ensure the one-sided evaluability of the contact. This data set is displayed in a boxplot for each joining stage. Thus, the interval of the process parameters, adjusted for outlier values, can be observed. In addition, the local joining process parameters are localised and optically interpreted for the MTC HX340LAD – EN AW-5182.

The local joining process parameters for the EN AW-5182–HX340LAD joint are shown in Fig. 7. As can

Table 7 Thermal properties of the simulated materials (λ = Thermal conductivity in (W/m*K), c = Specific heat capacity in (J/kg*K), α = Coefficient of thermal expansion in (10^{-5}))

Material	λ	c	α
HX340LAD	65	490	1.1
EN AW-5182	110	926	2.4
38B2 H4	65	490	1

be seen from the diagram, an interface pressure between $\sigma_N = 500 - 1500$ MPa affects the majority of the nodes in the evaluated process stages. Towards the end of the joining process (95% joining stroke), the interface pressure decreases significantly on average. In the observed stages, the interface pressure rises in some isolated nodes to almost $\sigma_N = 2800$ MPa. In addition, some nodes at every stage are present with very low interface pressures (close to $\sigma_N = 0$).

Furthermore, it can be seen that at the start of the process the relative velocity is in the range of $v_{rel} = 1-3$ mm/s. At this joining stage, the rivet is not yet bent up. Orthogonal penetration of the rivet into the sheet metal takes place.

In the second stage (50% joining stroke), the rivet spreads out and thus the relative velocity in the contact increases. In the subsequent stages, the relative velocity decreases again, so that at 95% joining stroke the relative velocity is already close to zero.

The temperature of the rivet nodes in contact has already risen to $T = 50$ °C on average at 25% joining stroke. As the riveting process progresses, the temperature rises up to $T = 200$ °C at 75% joining stroke. Towards the end of the process, the contact cools down again to approx. $T = 115$ °C on average. This occurs due to the rapid heat dissipation from the local joining point.

The local joining process parameters on the rivet in the joining process HX340LAD – EN AW-5182 are similar to the EN AW-5182 – HX340LAD joining process. The majority of the nodes in the contact exhibit interface pressures of $\sigma_N = 500-1500$ MPa across the process stages investigated. With regard to the relative velocity, the same pattern is revealed as with the other joint. The relative velocity is approx. $v_{rel} = 2$ mm/s at the start of the process and then increases up to $v_{rel} = 7$ mm/s (50 and 75% joining stroke) in the upper quartile as the process progresses, and drops significantly towards the end of the joining process. Similar to the other joint, the procedure of increasing relative velocity, which decreases again at the end of the process, can also be observed in the temperature. At the peak, temperatures of $T = 175$ °C can be observed in the third process stage. These process-related developments of the local joining process parameters are shown in Fig. 8 visual and in Fig. 9 in the boxplot representation. The plotted values for the local joining process parameters in Fig. 8 do not correspond to

the average values in the contact but to local areas. For the relative velocity these are indicated by using arrows.

From the numerically determined local joining process parameters, the relevant friction tests can be derived. The interface pressure is investigated above the initial yield point and over a wide interval, while the relative velocity is investigated in the considered interval as well as above, since the joining velocities in the real process can differ significantly. For the temperature, levels within the determined values from the joining processes were investigated.

3.2 Experimental investigations

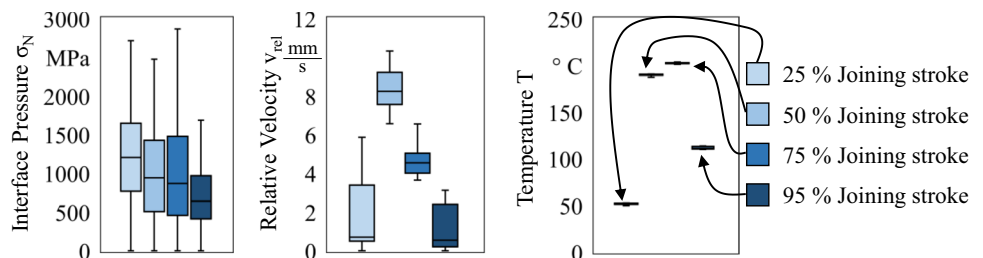
The result of a single friction test is the curve of frictional torque over twisting angle. With the help of geometry parameters, this can be represented as the friction coefficient μ or the frictional shear stress τ_f as a function of the frictional stroke s_f as shown in Fig. 10.

The mathematical formulas for the conversion from torque and rotation angle to frictional shear stress and frictional stroke are chosen analogously to Rossel et al. [11]. The curve initially shows a steep increase in the frictional shear stress towards static friction level. After the static friction has been overcome, it decays exponentially until it reaches a stationary state. This region is interpreted as dynamic friction. In the following sections, dynamic friction will be considered in more detail, because self-pierce riveting is a dynamic process as well.

The influence of the interface pressure is shown in Fig. 11. The diagram shows that the friction coefficient of the EN AW-5182—rivet contact decreases with increasing interface pressure. In addition, the standard deviation of the friction coefficient decreases with increasing interface pressure.

At an interface pressure of $\sigma_N = 50$ MPa, the friction coefficient is $\mu = 0.19295$. With an interface pressure of $\sigma_N = 400$ MPa, the friction coefficient already drops to $\mu = 0.14938$. At $\sigma_N = 700$ MPa, it drops further to $\mu = 0.13221$. The decrease of the friction coefficient is not linear, but along an exponential decay function. Contrary to the contact with EN AW-5182 in the contact between HX340LAD and the rivet, no clear dependence between friction coefficient and interface pressure emerges. An

Fig. 7 Boxplot representation of local joining process parameters on the rivet for different joining stages of the EN AW-5182 1.5 mm–HX340LAD 1.5 mm joint



interface pressure of $\sigma_N = 50$ MPa results in a friction coefficient of $\mu = 0.16$. At higher interface pressures, the friction coefficient fluctuates slightly above $\mu = 0.16$. It can be deduced that the friction coefficient for the contact between HX340LAD and rivet is independent of the interface pressure for the considered interval.

The stronger dependence on the interface pressure of EN AW-5182 is due to the greater deformation in the filigree sawtooth-shaped surface profile of aluminium. The zinc

layer of the steel material HX340LAD shows very massive peaks in the surface, so that the soft ALMAC[®]-coating flows around them rather than reshaping them at low interface pressures. The real contact area changes less as a result.

The Fig. 12 shows the development of the contact area with increasing interface pressure. At an increasing interface pressure of $\sigma_N = 50$ MPa, only a few traces of plastic deformation can be seen in the surface on the steel sheet. On the side of the rivet, the light zones show the areas of the surface

Fig. 8 Different process stages and local joining process parameters on the rivet of the HX340LAD 1.5 mm – EN AW-5182 1.5 mm joining process at 25, 50, 75 and 95% joining stroke

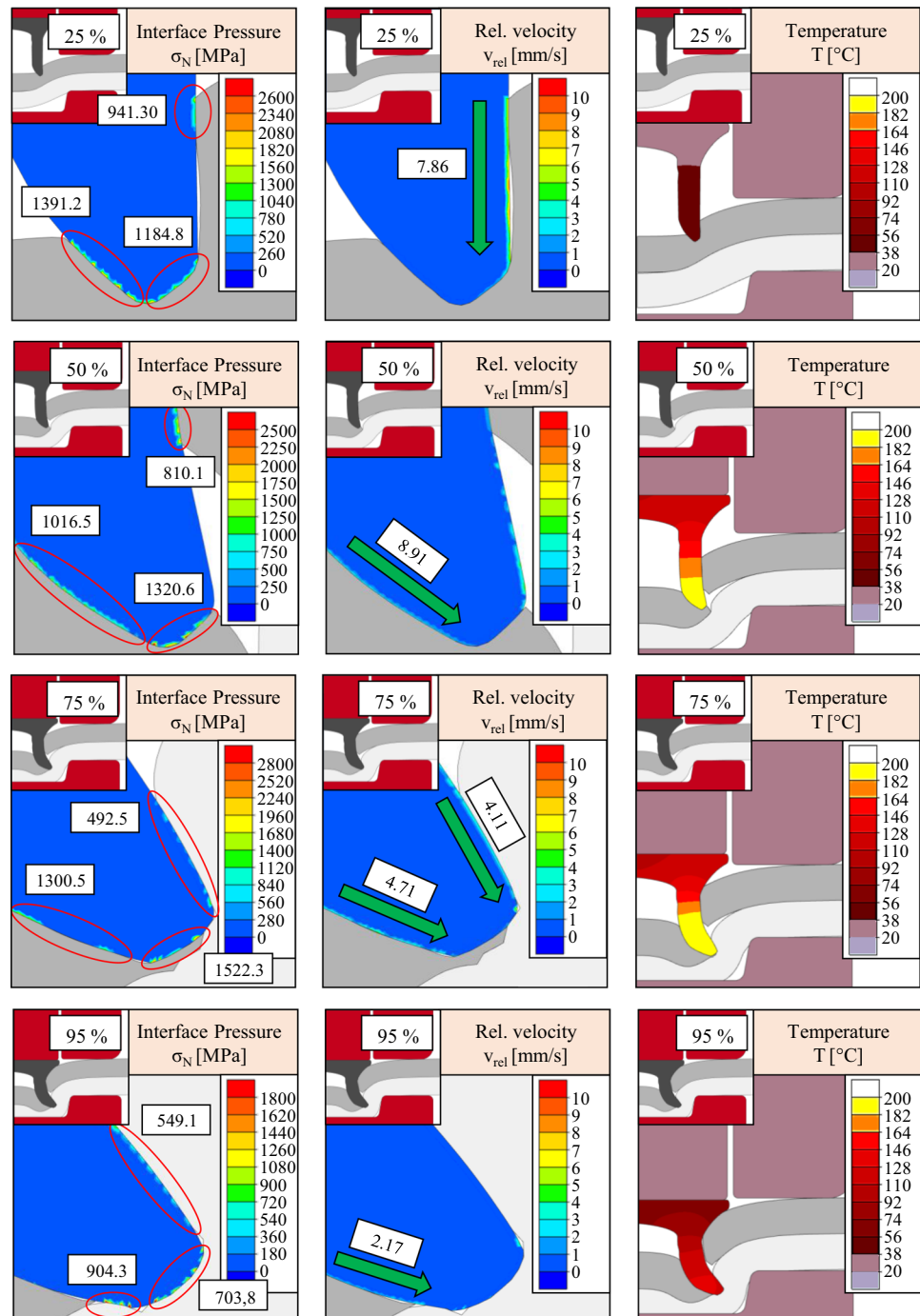


Fig. 9 Boxplot representation of local joining process parameters on the rivet for different joining stages of the HX340LAD 1.5 mm – EN AW-5182 1.5 mm joint

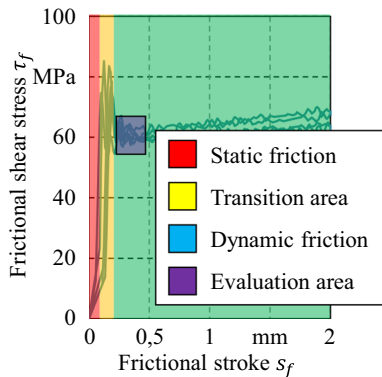
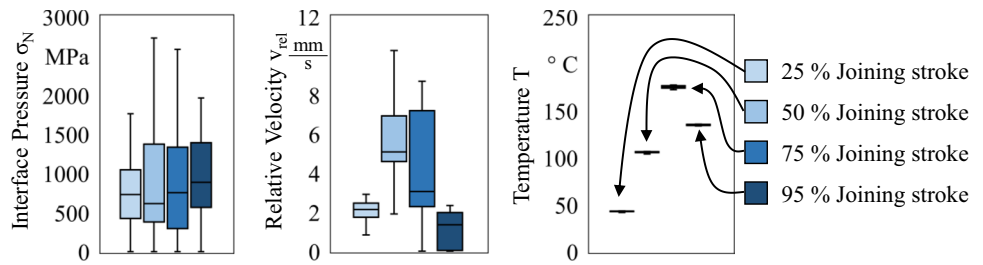


Fig. 10 Frictional shear stress as a function of the frictional stroke during the friction test

that was in contact during the friction test. At an interface pressure of $\sigma_N = 300$ MPa, the steel sheet shows clear traces of plastic deformation of the surface. These are more pronounced with increasing radius of the friction surface, since a greater frictional stroke is covered here. The same applies to the rivet surface, which shows a clear preferential direction from the friction test.

The results from the friction tests under variation of the relative velocity are shown in Fig. 13. The diagrams show that the effect of relative velocity on the friction coefficient is significant. Starting from a friction coefficient of $\mu = 0.17$ at $v_{rel} = 5$ mm/s, the friction coefficient increases continuously with increasing relative velocity. At $v_{rel} = 10$ mm/s, the friction coefficient is already at $\mu = 0.192$ and increases to $\mu = 0.2679$ at $v_{rel} = 20$ mm/s. Also for the contact between HX340LAD and the rivet, the relative velocity correlates

Fig. 11 Friction coefficient of different interface pressure levels for the contact of an ALMAC® coated semi-tubular self-pierce rivet C5,3×5,0 H4 with **a** EN AW-5182 and **b** HX340LAD

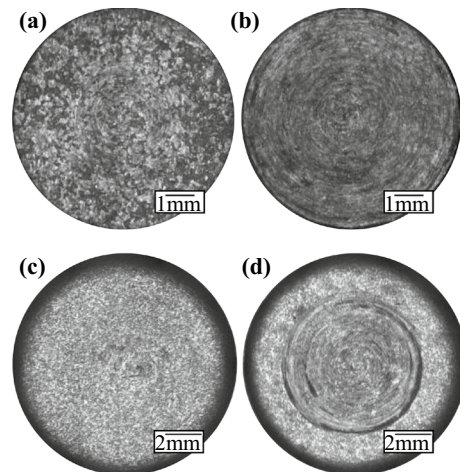
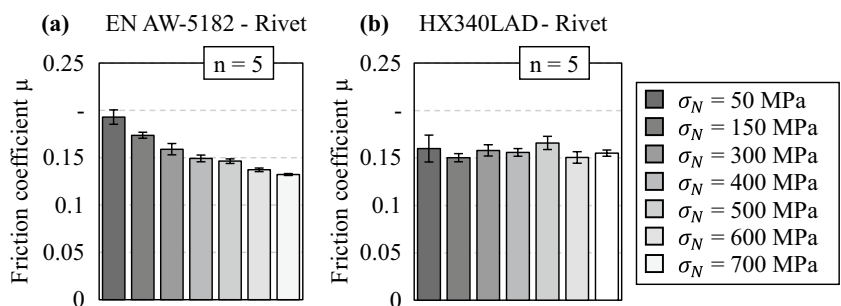
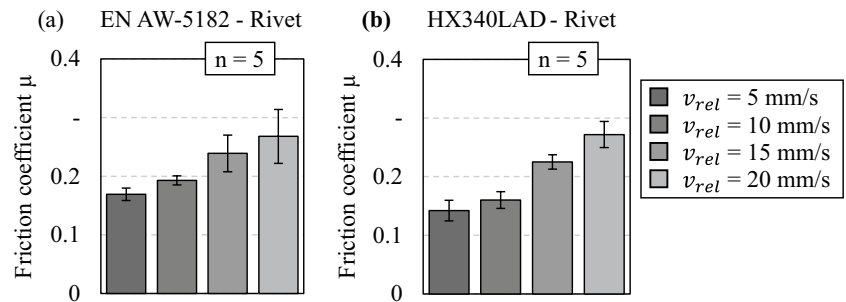


Fig. 12 Friction surface analysis after friction tests between rivet (a) and sheet (c) at $\sigma_N = 50$ MPa and rivet (b) and sheet (d) at $\sigma_N = 300$ MPa

positively with the friction coefficient. From $\mu = 0.142$ at $v_{rel} = 5$ mm/s, the friction coefficient increases to $\mu = 0.271$ at $v_{rel} = 20$ mm/s. This corresponds to an increase of approx. 90%. The effect of an increasing friction coefficient with increasing relative velocity at high interface pressures is also documented by Hora [13] with a rotational friction test bed. According to the stribeck curve, increasing friction indicates hydrodynamic friction. This implies a complete separation of the friction bodies by a lubricant. However, this can be ruled out due to the plastic deformation of the specimens. The behavior is therefore more likely to be due to inertial effects and micro-welding in the course of plastic

Fig. 13 Friction coefficient of different relative velocity levels for the contact of an ALMAC[®] coated semi-tubular self-pierce rivet C5.3×5.0 H4 with **a** EN AW-5182 and **b** HX340LAD



deformation of the contact surfaces. This hypothesis is also supported by the difficult separability of the friction partners after the friction test.

Additionally, the results of Westeneng [14] have shown that the relative velocity can influence the friction coefficient in different directions depending on the strain rate and visco elastic-behavior of the boundary layer. Further studies showed that the friction coefficient increases or decreases as a function of the velocity range [15].

The results for the temperature-dependent friction tests are shown in Fig. 14. It can be seen that for both materials EN AW-5182 and HX340LAD, contact with the rivet is associated with a temperature-related reduction of the friction coefficient. While the decrease in the contact between EN AW-5182 and rivet is lower at approx. 8% at $T = 150\text{ °C}$ compared to room temperature ($T = 20\text{ °C}$), the effect is way more significant in the contact with HX340LAD. There is a reduction in the friction coefficient of approx. 31% at $T = 150\text{ °C}$, starting from a temperature level of $T = 20\text{ °C}$. It is also noticeable that the friction coefficient at $T = 100\text{ °C}$ is slightly above the friction coefficient at $T = 50\text{ °C}$. If the standard deviation is taken into account, the tests at $T = 100\text{ °C}$ are still within the standard deviation of $T = 50\text{ °C}$. It can therefore be assumed that the experimental scatter is responsible for this, but the general trend of decreasing friction coefficients with increasing temperature is not affected. The significant impact of temperature on friction confirms the strong thermomechanical coupling in tribology mentioned in the literature [16]. The decreasing friction coefficient with increasing temperature

can be explained in terms of friction regimes in sheet metal forming: Boundary lubrication and ploughing [17]. During ploughing, the necessary frictional force results from the energy losses required during surface deformation. Thus, the friction coefficient depends directly on the material properties of the base material. The materials used exhibit a reduction in shear strength with increasing temperatures. Thus, a temperature-induced softening of the contact takes place [14]. The same applies to the boundary layer, which exhibits a reduced shear strength with increasing temperature in general [14].

With respect to the rivet coating, there is also a clear influence with regard to friction, as Fig. 15 shows. For both contacts with aluminium or steel, the ZnNi + B18 coating has a friction-reducing effect compared to ALMAC[®]. This occurs in harmony with the literature, as in [6] or [8], for example. An explanation is that the hardness of the ALMAC[®] coating is significantly lower than the ZnNi + B18 coating, so that plastic deformation in the surface layer area is included in the friction coefficient.

4 Summary

Overall, a numerical and experimental method was developed to identify the friction relevant local joining process parameters on the rivet, and an experimental method was developed to determine the friction coefficient in the relevant parameter spaces. On the part of the numerical joining process simulation, a friction subroutine was programmed and

Fig. 14 Friction coefficient of different temperature levels for the contact of an ALMAC[®] coated semi-tubular self-pierce rivet C5.3×5.0 H4 with **a** EN AW-5182 and **b** HX340LAD

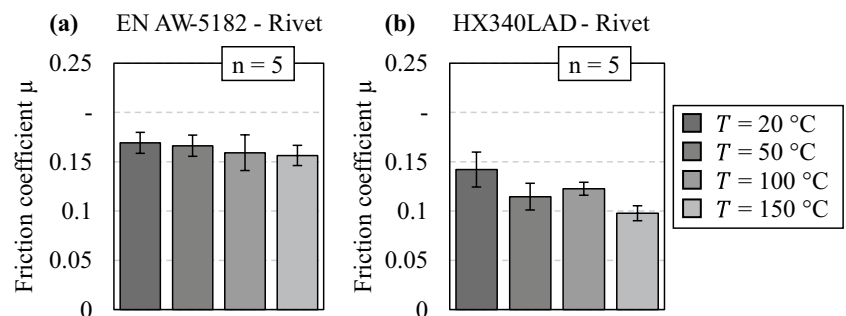
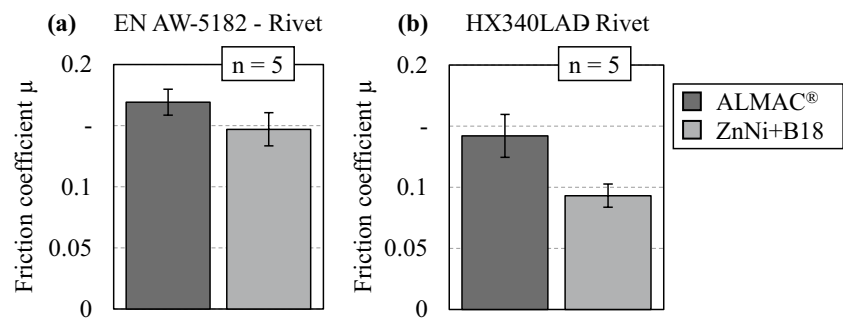


Fig. 15 Friction coefficient of different coatings for the contact of semi-tubular self-pierce rivet C5.3×5.0 H4 with **a** EN AW-5182 and **b** HX340LAD



evaluated in order to investigate the local joining process parameters in a special contact area in the joining process. Based on the results of the simulation, the boundary conditions for the experimental friction test were defined. In order to reproduce these boundary conditions as close as possible to the joining process, an experimental friction test bed was developed to reproduce the contact between the joining parts and the rivet. The test bed was subsequently used to carry out friction tests and identify elementary dependencies, which were then compared and discussed with comparable friction tests available in the literature.

Compared with other friction testing methods, the test bed presented in this paper allows to map the local joining process parameters closer to the joining process. In particular, with regard to the interface pressure, values above the initial yield point can be tested, which is not possible with a lateral kinematic due to plastic deformation. The temperature, which is a significant influence factor, can also be taken into account in the friction test.

The presented methodology provides the basis to experimentally parameterize a friction model close to the joining process and to increase the accuracy of numerical joining process simulations.

5 Outlook

In further investigations, the interdependent influences of the local joining process parameters on the friction can be studied. Further tests within the framework of a DoE-analysis are necessary for this. Other coatings can also be investigated. This is because the friction has a significant effect on the expansion behavior and the joint characteristics of the semi-tubular self-pierce riveted joint. Furthermore, other joining elements can also be investigated by making minor modifications to the test bed. Finally, the experimental friction results can parameterize a friction model for numerical joining process simulation and improve the accuracy of mechanical joining process simulations.

Acknowledgements The presented results are taken from IGF research project 20235 N by the European Research Association for Sheet Metal Working (EFB), which has been funded by the German Federation of Industrial Research Associations (AiF) under the program for promotion of industrial research (IGF) (IGF no. 20235 N) by the Federal Ministry for Economic Affairs and Energy (BMWi) based on a decision of the German Bundestag.

Funding Open Access funding enabled and organized by Projekt DEAL.

Open Access This article is licensed under a Creative Commons Attribution 4.0 International License, which permits use, sharing, adaptation, distribution and reproduction in any medium or format, as long as you give appropriate credit to the original author(s) and the source, provide a link to the Creative Commons licence, and indicate if changes were made. The images or other third party material in this article are included in the article's Creative Commons licence, unless indicated otherwise in a credit line to the material. If material is not included in the article's Creative Commons licence and your intended use is not permitted by statutory regulation or exceeds the permitted use, you will need to obtain permission directly from the copyright holder. To view a copy of this licence, visit <http://creativecommons.org/licenses/by/4.0/>.

References

- Han SL, Tang XD, Gao Y et al (2015) Effects of friction factors on flat bottom self-pierce riveting joints of AZ31 magnesium alloy. *Mater Res Innov* 19:S10-235-S10-238. <https://doi.org/10.1179/1432891715Z.0000000002155>
- Li D (2017) Influence of aluminium sheet surface modification on the self-piercing riveting process and the joint static lap shear strength. *Int J Adv Manuf Technol* 93:2685–2695. <https://doi.org/10.1007/s00170-017-0710-6>
- Han L, Chrysanthou A, Young KW (2007) Mechanical behaviour of self-piercing riveted multi-layer joints under different specimen configurations. *Mater Des* 28:2024–2033. <https://doi.org/10.1016/j.matdes.2006.06.015>
- Ang HQ (2021) An overview of self-piercing riveting process with focus on joint failures, corrosion issues and optimisation techniques. *Chin J Mech Eng.* <https://doi.org/10.1186/s10033-020-00526-3>
- Karim MA, Jeong T-E, Noh W et al (2020) Joint quality of self-piercing riveting (SPR) and mechanical behavior under the frictional effect of various rivet coatings. *J Manuf Process* 58:466–477. <https://doi.org/10.1016/j.jmapro.2020.08.038>

6. Wituschek S, Kuball CM, Merklein M et al (2020) Test method for friction characterization of rivets. DDF 404:132–137. <https://doi.org/10.4028/www.scientific.net/ddf.404.132>
7. Böhnke M, Rossel M, Bielak CR et al (2021) Concept development of a method for identifying friction coefficients for the numerical simulation of clinching processes. *Int J Adv Manuf Technol*. <https://doi.org/10.1007/s00170-021-07986-4>
8. Uhe B, Kuball CM, Merklein M et al (2021) Influence of the rivet coating on the friction during self-piercing riveting. *KEM* 883:11–18. <https://doi.org/10.4028/www.scientific.net/KEM.883.11>
9. Gavrilu M, Millet JP, Mazille H et al (2000) Corrosion behaviour of zinc–nickel coatings, electrodeposited on steel. *Surf Coat Technol* 123:164–172. [https://doi.org/10.1016/S0257-8972\(99\)00455-7](https://doi.org/10.1016/S0257-8972(99)00455-7)
10. Rossel M, Meschut G (2022) Increasing the accuracy of clinching process simulations by modeling the friction as a function of local joining process parameters. *Proc IMechE Part L: J Materials: Des Appl*. <https://doi.org/10.1177/14644207221074290>
11. Rossel M, Böhnke M, Bielak C et al (2021) Development of a method for the identification of friction coefficients in sheet metal materials for the numerical simulation of clinching processes. *KEM* 883:81–88. <https://doi.org/10.4028/www.scientific.net/KEM.883.81>
12. Piott M, Werber A, Schleuss L et al (2020) A study of the heat transfer mechanism in resistance spot welding of aluminum alloys AA5182 and AA6014. *Int J Adv Manuf Technol* 111:263–271. <https://doi.org/10.1007/s00170-020-05650-x>
13. Hora P, Gorji M, Berisha B (2011) Modeling of friction phenomena in extrusion processes by using a new torsion-friction test. *KEM* 491:129–135. <https://doi.org/10.4028/www.scientific.net/KEM.491.129>
14. Westeneng JD (2001) Modelling of contact and friction in deep drawing processes, Enschede. <https://research.utwente.nl/en/publications/modelling-of-contact-and-friction-in-deepdrawing-processes>
15. Bar-Sinai Y, Spatschek R, Brener EA et al (2014) On the velocity-strengthening behavior of dry friction. *J Geophys Res Solid Earth* 119:1738–1748. <https://doi.org/10.1002/2013JB010586>
16. Vakis AI, Yastrebov VA, Scheibert J et al (2018) Modeling and simulation in tribology across scales: an overview. *Tribol Int* 125:169–199. <https://doi.org/10.1016/j.triboint.2018.02.005>
17. Shisode M, Hazrati J, Mishra T et al (2021) Modeling boundary friction of coated sheets in sheet metal forming. *Tribol Int* 153:106554. <https://doi.org/10.1016/j.triboint.2020.106554>

Publisher's Note Springer Nature remains neutral with regard to jurisdictional claims in published maps and institutional affiliations.